Calculations of inlet distortion induced compressor flow field instability

R. Chue*, T. P. Hynes†, E. M. Greitzer*, C. S. Tan*, J. P. Longley†
*Gas Turbine Laboratory, Massachusetts Institute of Technology, Cambridge, MA, USA
†Whittle Laboratory, Cambridge University, Cambridge, UK

Calculations of the onset of flow instability are presented for low speed multistage axial compressors operating with asymmetric inlet flow. The most important feature of the calculation procedure is the modeling of the fluid dynamic interaction between the spoiled and unspoiled sectors of the compressor. The calculations show that annulus averaged slope of the compressor pressure rise characteristic equal to zero is a useful approximate stability criterion for situations where the dynamics of the compressor flow field do not couple strongly to the compression system *or* the structure of the imposed distortion is not similar to that of the eigenmodes of the flow in the compressor annulus. This approximate criterion is used to investigate the relationship between the present model and the "parallel compressor" model. Calculations are also performed for cases of interest when compressor and compression system *are* closely coupled, as well as situations in which the compressor is subjected to a rotating distortion. (This would occur, for example, in a two-spool engine with the low compressor in rotating stall.) These first-of-a-kind computations, and the accompanying description of the physical mechanisms, show that the stability of the flow in the compressor can be adversely affected if the temporal or spatial structure of the distortion is such that resonant type responses can be evoked either from the compressor or from compressor/compression system interactions.

Keywords: axial compressor flow stability; inlet flow distortion; rotating stall; surge; unsteady flows in axial compressors

Introduction

The adverse effects on gas turbine engine operation due to inlet distortion are well known and need no detailed introduction. Because of its consequences, the distortion problem has received considerable attention, and a large amount of experimental and theoretical work has been conducted on the topic.

The most critical aspect is assessment of the effect on the stability of flow in the compressor due to a given inlet distortion. In a previous paper,[1] a new method was presented for computing this loss in stability by examining the conditions under which small disturbances, which propagate round the annulus, will grow. The analysis, which appears to be the first to treat this problem from the point of view of a rigorous fluid dynamic instability calculation, showed trends in compressor behavior in good agreement with existing experimental observations.

A key feature of the method is the ability to account properly for the interaction between the high and low total pressure sectors of the compressor. As discussed below, it is this, rather than any "critical residence time in the distorted region," that is important in determining the stability of the distorted flow. To analyze the flow instability that occurs in the presence of this interaction, the small perturbations are imposed on a time mean flow that is circumferentially strongly nonuniform. The "background" flow field is thus a nonlinear disturbance (distortion) whose calculation is itself a part of the overall computation procedure.

In Ref. 1 the emphasis was in describing the method and presenting initial computations showing the type of results that could be obtained. That paper thus included only brief discussion of the structure of the disturbances, the question of the existence of a simple overall criterion for instability, the relation between the computational results and previous attempts to deal with this problem, such as the "parallel compressor" method, and the basic physical mechanisms that are associated with the observed behavior.

The present paper covers these aspects as well as examines several phenomena which have not been previously discussed theoretically. The first of these is the coupling due to resonance between the propagating type of flow disturbances which characterize the *compressor* and the overall pulsations associated with the *compression system*. A necessary condition for this coupling is a nonuniform background flow. The second is another type of resonance that can exist between the inlet distortion and the disturbances in the compressor annulus, with the former acting as a forcing function for the latter. The general trend in both these situations is that the stable flow range is decreased, so that they are of interest from an engineering standpoint. Physical explanations are given for the observed behavior.

The emphasis here is on the basic fluid phenomena, rather than extensive parametric studies. However, an examination is also made of the impact on the predictions of some of the different loss models that have been proposed for describing the unsteady processes within the compressor blade passages. This is useful for assessing the importance of this aspect of the modeling.

Address reprint requests to Professor Greitzer at 31-264, Gas Turbine Laboratory, Massachusetts Institute of Technology, Cambridge, MA 02139, USA.

Received 3 October 1987; accepted 2 February 1989

Brief description of the model

Because of the detailed description given in Ref. 1, only a brief review of the model will be presented here. A listing of the relevant assumptions and equations is given in the appendix. For calculations of the compressor performance, we assume a low speed compressor of sufficiently high hub-to-tip ratio that a two-dimensional treatment is valid. The pressure rise across any blade row in the compressor is taken to be made up of that achieved in steady uniform flow at the local entry conditions plus that necessary to balance the acceleration of the fluid within the blade row.[2] When the contributions from each blade row are added, this implies a pressure rise across the *whole compressor* of (at each value of θ),

$$\frac{P_2-P_{t_1}}{\rho U^2}=\psi(\phi)-\lambda\frac{\partial\phi}{\partial\theta}-\frac{\mu r}{U}\frac{\partial\phi}{\partial t} \tag{1}$$

In Equation 1, P_2 and P_{t_1} are the static pressure at compressor exit and the total pressure at the compressor inlet; the parameters λ and μ, which are defined in the Appendix, represent the inertia of the fluid in the rotors and in all blade rows respectively; ϕ is the local value of axial flow coefficient ($\phi=C_x/U$); and ψ is the inlet total to exit static pressure rise characteristic under uniform flow conditions at the local value of ϕ. ψ is assumed to be a smooth continuous function of flow coefficient and, again, is the performance that would be obtained if the flow through the compressor were steady and axisymmetric, i.e., the blade element performance free from rotating stall. An examination of the form of ψ for a three-stage compressor has recently been made by Longley.[3,4] Unless otherwise specified, the particular form used for ψ in the calculations presented herein is that shown in Figure 1, which is based on parameters from a low speed three-stage compressor.[5] Its explicit form is given below. Equation 1, which expresses the local pressure rise across the compressor as a function of the local axial velocity, must be combined with a description of the upstream and downstream flow fields and of the overall system in which the compressor operates, as will be discussed below.

The problem of assessing the effect of inlet distortion on the stability of the flow through the compressor is inherently a nonlinear one. A central concept in the present approach is that the strong nonlinearity of the compressor performance (ψ, as a function of flow coefficient ϕ) has the greatest importance,[1] so this is treated in a fully nonlinear manner.

To solve Equation 1, the pressure terms must be related to $\phi(\theta,t)$. This involves the calculation of the flow fields upstream and downstream of the compressor and is also a nonlinear problem. We regard the nonlinearities associated with the flow

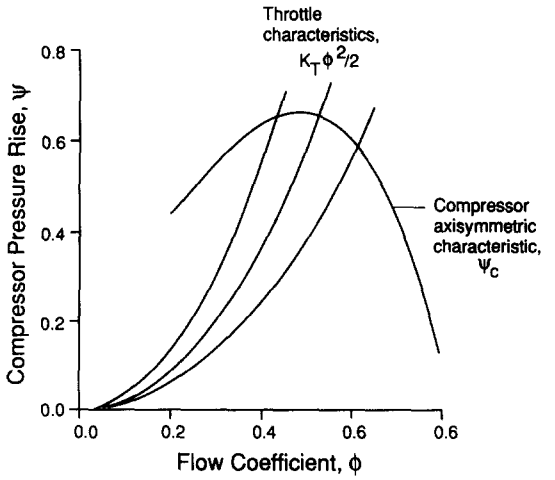

Figure 1 Compressor and throttle characteristics used in examples

Notation

a	Speed of sound; also used in definition of parabolic compressor characteristic
A_n	Fourier coefficients of axial velocity perturbation at compressor face
A	Flow-through area
b_x	Axial chord
B	Nondimensional system parameter; $B=(U/2a)\sqrt{V_{\text{plenum}}/AL_{\text{TOT}}}$
C_x	Axial velocity
f	Distortion angular velocity (fraction of rotor rotation rate)
K_t	Throttle setting coefficient
k	Harmonic number
L	Blade row loss characteristic
L_{TOT}	Overall effective length of compressor and compressor ducting
N	Number of stages
P	Static pressure
P_t	Total pressure
r	Mean radius
R_L	Pressure rise in distorted sector
t	Time
$\tilde{T}'$	Nondimensional slope of throttle pressure drop characteristic
U	Wheel speed
V_{plenum}	Volume of plenum
γ	Stagger angle
$\delta(\ )$	Perturbation quantity
η	Nondimensional effective length $=L_{\text{TOT}}/r$
λ	Inertia parameter (rotors)$=\sum b_x/r\cos^2$(stagger)
μ	Inertia parameter (all blade rows)$=\sum b_x/r\cos^2\gamma$
τ_L	Unsteady loss parameter (nondimensional)
ϕ	Axial velocity coefficient; $\phi=C_x/U$
ϕ	Annulus averaged axial velocity coefficient
ψ	Nondimensional compressor pressure rise in axisymmetric flow; $\psi=(P_2-P_{t_1})/\rho U^2$
ω	Radian frequency of perturbation
ω_H	Helmholtz resonator frequency
θ	Circumferential angle
ρ	Density

Subscripts

0	Inlet to compressor duct
1	Compressor inlet
2	Compressor exit
3	Plenum inlet
4	Throttle outlet
R	Rotor
S	Stator
SS	Steady state
m	Value at peak pressure rise (parabolic characteristic)
ID	Ideal pressure rise with no losses

field as much less important than those associated with the compressor performance, and the equations used upstream and downstream of the compressor are thus taken to be those for linear perturbations about a uniform flow. This approximation for treating the flow field has in fact been shown by several authors, e.g., Refs. 6 and 7, to be a good one in the present context. Further discussion of this approach and its justification can be found in Ref. 1; a different point of view is given in Ref. 8.

Because the background flow is nonuniform, the unsteady flow field perturbations that we are considering (i.e., the eigenmodes of the system) do not have a purely sinusoidal distribution round the annulus. In addition, the instantaneous annulus averaged mass flow is not in general zero, as it would be, for example, for propagating disturbances on a uniform background flow. The latter implies that the *global* compression system behavior is coupled to the *local* compressor behavior, so that a description of the overall compression system, as well as the compressor flow field, must thus be included in the model.

The compression system studied is modeled as a compressor pumping to a plenum, which exhausts through an ideal throttle. The length of the compressor ducting is taken as long enough so there are no nonaxisymmetric potential flow interactions with the inlet and exit duct terminations. This is not a limitation of the theory, but is adopted only to simplify the algebra. Density changes in the plenum are related to pressure changes through an isentropic relationship and the inertia of the fluid in the throttle is neglected. The nondimensional parameters which characterize the compressor and system dynamic behavior are[1]

$$\eta=\frac{L_{\mathrm{TOT}}}{r}=\frac{\text{effective compressor length}}{\text{mean radius}}$$

and

$$B=\frac{U}{2a}\sqrt{\frac{V_{\mathrm{plenum}}}{AL_{\mathrm{TOT}}}}$$

The axisymmetric compressor pressure rise characteristic, $\psi(\phi)$, must also be specified. Pressure rise here is defined from inlet total to exit static pressure, and the explicit shape of the curve used in the computations is taken as $\psi=-5.76\phi^3+4.32\phi^2+0.3$. This is consistent with data from a low speed, three-stage compressor,[5] and should be a reasonable generic representation.

To complete the formulation of the problem, some way of specifying the inlet distortion must be added. In many practical situations, the flow through the compressor can influence the flow through the distortion generator.[1] This, however, is a complication of detail rather than of principle and we do not address it here. We thus assume that the total pressure distortion is specified as a function of θ (and sometimes also t) at a location which is upstream of the asymmetric static pressure field ahead of the compressor.

Calculation procedure for the background flow

Once the inlet distortion is specified, a solution to Equation 1 can be found. If the distortion is steady, Equation 1 reduces to a nonlinear ordinary differential equation for the background flow,

$$\frac{P_2(\theta)-P_{t_1}(\theta)}{\rho U^2}=\psi[\phi(\theta)]-\lambda\frac{\mathrm{d}\phi}{\mathrm{d}\theta} \tag{2}$$

The linearized treatment of the upstream and downstream flow fields implies that $P_{t_1}(\theta)$ is the same as the specified far upstream total pressure distortion. For a steady distortion, a steady solution is demanded for the background flow. Another case, discussed later, is that of a rotating distortion; in this case, a background solution which rotates at the prescribed frequency is sought.

There are various ways of obtaining the desired solution; we have elected to use a Fourier collocation (or pseudospectral) method,[9] which exploits the circumferential periodicity of the flow. The flow variables are thus represented as

$$\phi=\sum_{k=-K}^{K-1}A_k(t)e^{ik\theta}$$

so that the steady-state equations are exactly satisfied at $2K+1$ points around the annulus. The Fourier coefficients are solved for using a preconditioned Newton's iterative method to obtain an optimum convergence rate. Nonlinear terms are evaluated by direct multiplication of discretized functions in physical space while differentiation is done in the Fourier space. Whichever way the computation is carried out, however, the important point is that a steady solution can be obtained for the background flow and that, as is general in hydrodynamic stability problems, it can be obtained whether or not such a flow would be stable in practice.

Stability assessment

The issue of stability is decided by a separate calculation. To the background flow is added an arbitrary small, unsteady perturbation. If any such perturbation grows with time, the flow through the compressor is adjudged unstable; only if all possible solutions decay with time is stability assured. Linearization about the flow field given by Equation 1 yields an equation for the perturbation quantities, denoted by $\delta(\ )$:

$$\frac{\delta P_2-\delta P_{t_1}}{\rho U^2}=\frac{\mathrm{d}\psi}{\mathrm{d}\phi}\delta\phi-\lambda\frac{\partial\delta\phi}{\delta\theta}-\frac{\mu r}{U}\frac{\partial\delta\phi}{\delta t} \tag{3}$$

The local value of the slope of the compressor characteristic, $\mathrm{d}\psi/\mathrm{d}\phi$, will generally be a strong function of θ, and solutions of this equation can thus differ markedly from the purely sinusoidal solutions obtained in undistorted flow (where $\mathrm{d}\psi/\mathrm{d}\phi$ is constant around the annulus).

The small perturbation approach is a standard technique in stability theory and represents in effect an eigenmode and eigenvalue problem. In physical terms, the unsteady perturbations to the flow may be viewed as incipient stall cells when they propagate around the annulus and as small amplitude, surge-like system transients when they are predominantly one-dimensional in character.

Structure of the disturbance mode

To understand the overall behavior of the compressor/compression system, it is useful first to examine the structure of the eigenmode at the onset of instability. The perturbations of flow quantities at the compressor face are of the form

$$\delta(\ )=\sum_k A_k e^{i(k\theta+\omega t)} \tag{4}$$

with the value of ω determined from the stability analysis. If ω has a negative imaginary part, growth of the disturbance is implied and the flow is unstable.

The components of the solution eigenvectors are the Fourier components, A_k, for the spectral representation of the axial velocity perturbation, the plenum pressure, δp, and the throttle mass flow perturbations, which correspond to that particular

eigenmode. The individual eigenmodes will generally have a rich harmonic content. The form of the eigenmodes is different when the compressor and the compression system are not strongly coupled compared to when a strong coupling exists, and we thus examine behavior in both cases, starting with the former situation. The distortion used is a square wave of 120° extent; this is representative of distortion employed in compressor testing.

The nomenclature to be followed is to call the single lobed disturbance the first eigenmode, the disturbance with two lobes the second eigenmode, the disturbance which has its zeroth Fourier component largest the zeroth mode, etc. One can (loosely) view the zeroth eigenmode as a surge-like disturbance and the others as different order propagating stall-like disturbances. The coupling between different harmonic components in each eigenmode is strongest for the near neighbors, because the imposed distortion has as its strongest component the first harmonic. This is true for most distortions that are of practical interest in the present context, i.e., those which have a significant effect on the stall point. In addition, the eigenmode corresponding to the single lobe has been found to be most critical for instability and we will discuss this as typifying the general behavior to be found.

Even though the nearest neighbor relationship remains as the parameters that characterize the system are varied, other aspects of the behavior do change considerably. One reason for this can be seen by considering the frequencies characterizing the different eigenmodes. The velocity of propagating disturbances essentially scales with the rotor speed and is not much affected by system (plenum volume, overall compressor length) parameters. The frequency of the surge-like type of disturbance, however, is not very dependent on rotor speed but is set by the system dimensions.

As B is changed, the ratio of the two frequencies also changes and, for a particular value of B, the two will coincide as shown in Figure 2. In the figure, the frequencies of the surge-like and one-lobed propagating eigenmodes are plotted versus B. For the parameters listed, the two frequencies coincide at $B=0.34$. In the figure, two sets of curves are shown: the solid curves are from computations with a large amplitude inlet distortion (the difference between high and low total pressure regions corresponds to roughly 1.5 times the dynamic pressure based on the mean velocity). The dashed curves show the frequencies for a situation with uniform inlet (no distortion), based on analyses for rotating stall and surge under uniform flow conditions.[2,10]

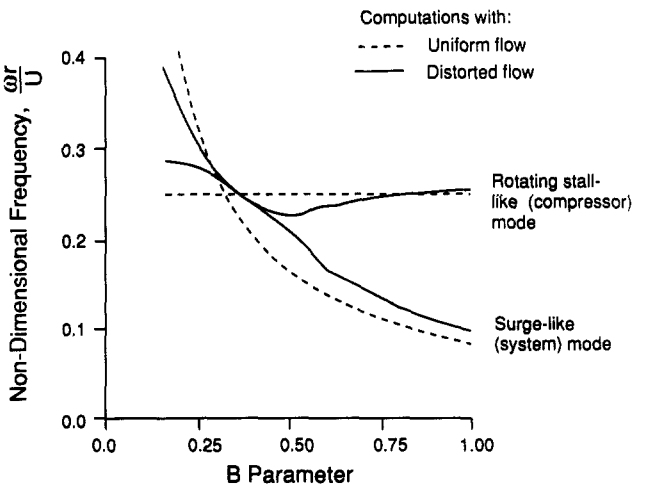

Figure 2 Frequencies of rotating stall-like and surge-like eigenmodes at neutral stability (stall point) with uniform flow and with inlet distortion; $\eta=6$, $\lambda=1$, $\mu=2$, 120° extent distortion, $\Delta P_t/\rho U^2=0.2$

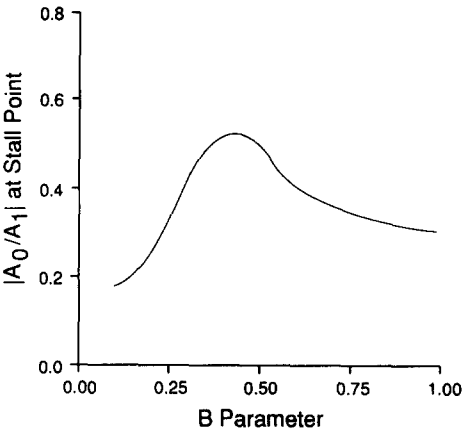

Figure 3 Ratio of Fourier components of compressor eigenmode at neutral stability point; $\eta=6$, $\lambda=1$, $\mu=2$, 120° extent distortion, $\Delta P_t/\rho U^2=0.2$

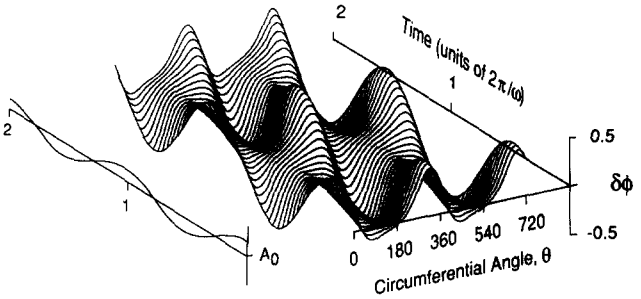

Figure 4 Structure of compressor eigenmode near resonance showing annulus averaged mass flow fluctuations (A_0 component) versus time; $\eta=6$, $\lambda=1$, $\mu=2$, 120° extent distortion, $\Delta P_t/\rho U^2=0.2$

As shown by Longley,[3] even for this large distortion, there is little effect on the disturbance frequencies, and this property will be made use of in some of the physical arguments given below.

In the neighborhood of frequency coincidence, the coupling between the zeroth and first Fourier components becomes stronger, as seen in Figure 3, which shows the ratio of the zeroth and first harmonic components of the first (propagating stall-like) eigenmode. Away from coincidence, the first harmonic dominates, but this is less true in the neighborhood of coincidence.

The change in the structure of the eigenmodes is not the only phenomenon that occurs in the neighborhood of coincidence. A more direct effect is an alteration in the stability boundary. More specifically, when the frequencies approach one another, the flow in the compressor becomes unstable at a higher flow rate than when the two frequencies are far apart. This will be taken up in a subsequent section, where it will be shown that the stability is due to a resonance between propagating and system type frequencies.

As a prelude to the general discussion that follows, it is of interest to look at the time domain representations of the eigenmodes. Figure 4 thus presents a plot of axial velocity perturbation, $\delta\phi$, versus circumferential angle, θ, at different times for a situation near this resonance, i.e., near the frequency coincidence. Two periods are shown in both θ and time, so that the motion of the wave can be seen more clearly. The eigenmode shown is the most unstable one (the first), and the conditions are taken at the neutral stability point. The figure is normalized with respect to the maximum peak-to-peak axial velocity perturbation. As implied in Ref. 1, there is considerable variation of the wave shape as it propagates round the annulus

(this occurs both near the resonance and far from it). At resonance, there is also a strong fluctuation in annulus averaged mass flow which, for this case, is roughly 25% of the maximum perturbation in $\delta\phi$.

With this discussion of the nature of the eigensolutions as background, we can now turn to some of the results concerning stability. We first examine the situation away from resonance where a simple criterion for instability can be derived.

Comments on a general stability criterion for distorted flow

In Ref. 1, it was suggested that the point of instability for a compressor in a steady, circumferentially distorted flow would occur when the area averaged value of the compressor characteristic slope or integrated mean slope (IMS) was zero,

$$\frac{1}{2\pi}\int_0^{2\pi}\frac{d\psi}{d\phi}\,d\theta=0 \tag{5}$$

The integrand here is evaluated using the background steady distorted flow, given by solving Equation 2 along with the relevant boundary conditions. The suggestion was made based on the results of applying the perturbation stability analysis to a variety of different distortion/compression system combinations. Varied quantities included: compressor characteristic; shape, extent, and amplitude of the distortion; system dynamics parameters B and η; and blade row inertia parameters λ and μ. Over a wide range of parameters, Equation 5 was found to hold at the instability onset operating point with surprising accuracy.

A heuristic argument for the validity of Equation 5 can be based upon a simplified treatment of Equation 3. If we make the assumption that (as the numerical calculations show) the most important term in the expression for upstream and downstream pressure fluctuations is the first harmonic component, Equation 3 can be written in terms of the axial velocity perturbation, $\delta\phi$, as

$$\frac{\mu r}{U}i\omega\delta\phi+\lambda\frac{\partial\delta\phi}{\partial\theta}-\left(\frac{d\psi}{d\phi}\right)\delta\phi-2i\frac{\omega r}{U}\delta\phi=0 \tag{6}$$

The solution of Equation 6 has the general form

$$\delta\phi=g(\theta)e^{i\omega t}$$

where

$$\frac{dg}{d\theta}+\frac{1}{\lambda}\left(i\mu\frac{\omega r}{U}-2i\frac{\omega r}{U}-\frac{d\psi}{d\phi}\right)g=0$$

The function $g(\theta)$ is given by

$$g(\theta)=\exp\left(\frac{1}{\lambda}\int_0^{\theta}\frac{d\psi}{d\phi}\,d\theta'-\frac{i\mu}{\lambda}\frac{\omega r}{U}\theta-2i\frac{\omega r}{U}\theta\right)$$

Since ϕ must be periodic as a function of θ, the argument of the exponential must take the value $2\pi iM$ for some integer M, and this condition determines the eigenvalue ω. At the neutral stability operating point, ω is purely real. Equation 5 thus follows. Solutions to Equation 6 can be written as

$$\delta\phi=\exp\left(\frac{1}{\lambda}\int_0^{\theta}\frac{d\psi}{d\phi}\,d\theta'+iM\left(\theta-\frac{\lambda U/r}{\mu+2}t\right)\right) \tag{7}$$

This shows explicitly that the axial velocity perturbation has the form of a wave traveling round the annulus with amplitude exponentially increasing in regions where $d\psi/d\phi$ is positive, and exponentially decaying in regions where $d\psi/d\phi$ is negative. From this point of view, the situation can be regarded as a balance between locally stable and unstable sectors of the annulus.

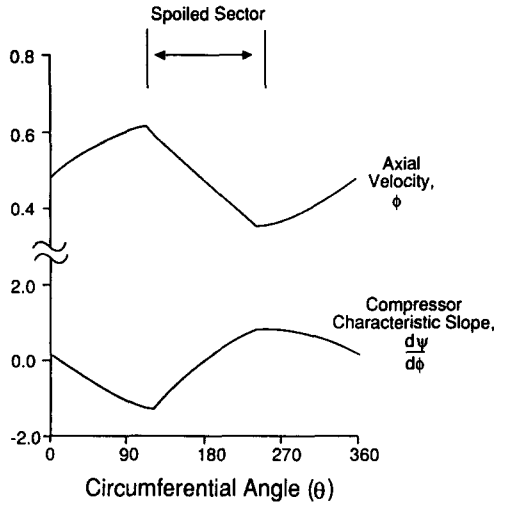

Figure 5 Local time mean "background" flow variables at compressor inlet versus circumferential position; $B=1$, $\eta=6$, $\lambda=1$, $\mu=2$, 120° extent distortion, $\Delta P_t/\rho U^2=0.2$

Because the compressor characteristic slope, $d\psi/d\phi$, can vary markedly over different parts of the annulus, the growth and decay rates can be large in practical situations. As an example, Figure 5 shows the time mean (background) axial velocity and compressor characteristic slope, $d\psi/d\phi$, for a square wave distortion of 120° extent. The operating condition is at neutral stability. Both ψ and $d\psi/d\phi$ are essentially in quadrature with the total pressure distortion (the "spoiled sector"), because of the dominance of local unsteady effects at operating points near the peak of the compressor characteristic.

The analysis given above provides a plausibility argument for the use of IMS equal to zero as a stability criterion, but it is stressed that it is the large body of more rigorous computations which underpins our belief in its applicability. There are, however, a number of similarities between the perturbations computed using the full analysis and the approximate expression of Equation 7. The regions of the annulus where the calculated perturbation amplitude grows and where it decays correlate well with the sign of $d\psi/d\phi$. All traveling wave-type of disturbances appeared to become unstable together (as is the case in Equation 7). Finally, those cases where IMS=0 was found not to apply were cases where the validity of the heuristic argument might be questioned: these are discussed subsequently.

Applications of the integrated mean slope criterion and connection with parallel compressor theory

The IMS=0 criterion is, when valid, a very useful result, as one can compute the instability point in a simple manner. We can exploit this criterion to examine the importance of parameters such as λ (compressor blade row inertia parameter). We will deal with a mathematically simple situation and take the compressor characteristic to be a parabola. Other shapes can readily be dealt with at the expense of algebraic complexity but this is a useful approximation which has generic behavior near the peak. Thus:

$$\psi=\psi_m-a^2(\phi-\phi_m)^2$$

The stability criterion IMS = 0 becomes

$$0 = \int_0^{2\pi} -2a^2(\phi - \phi_m)\, d\theta$$

that is

$$\bar{\phi} = \phi_m \tag{8}$$

For an inlet distortion of square wave type, as shown in Figure 7, the equation that determines the distribution of ϕ round the annulus, Equation 1, becomes

$$\lambda \frac{d\phi}{d\theta} = \psi_m - R_L - a^2(\phi - \phi_m)^2 \tag{9}$$

In Equation 9, R_L is the overall pressure rise in the low total pressure ($\theta < \theta^-$) sector of the annulus. In the high total pressure sector ($2\pi > \theta > \theta^-$), we have

$$\lambda \frac{d\phi}{d\theta} = \psi_m - R_L + \frac{\Delta P_t}{\rho U^2} - a^2(\phi - \phi_m)^2 \tag{10}$$

Examination of the sign of $d\phi/d\theta$ in the distorted sector implies, from Equation 9, that $R_L > \psi_m$.

Equations 9 and 10 can be solved to obtain ϕ as a function of θ:

$$\phi = \phi_m - \left(\frac{1}{a}\right)(R_L - \psi_m)^{1/2} \tan\left[\left(\frac{a}{\lambda}\right)(R_L - \psi_m)^{1/2}\left(\theta - \frac{\theta^-}{2}\right)\right]$$

$$\theta < \theta^- \tag{11a}$$

and

$$\phi = \phi_m - \left(\frac{1}{a}\right)\left(\psi_m + \frac{\Delta P_t}{\rho U^2} - R_L\right)^{1/2} \times \tanh\left[\left(\frac{a}{\lambda}\right)\left(\psi_m + \frac{\Delta P_t}{\rho U^2} - R_L\right)^{1/2}\left(\pi - \theta + \frac{\theta^-}{2}\right)\right]$$

$$2\pi > \theta > \theta^- \tag{11b}$$

The low total pressure sector pressure rise, R_L, at neutral stability is determined by the IMS = 0 condition that $\bar{\phi} = \phi_m$.

From Equation 11a, if ϕ is to remain finite in the θ^- sector, $[(a/\lambda)(R_L - \psi_m)^{1/2}](\theta^-/2)$ must not exceed $\pi/2$. This condition, and the condition that $R_L > \psi_m$ mentioned previously, imply

$$\psi_m < R_L < \psi_m + \frac{\pi^2 \lambda^2}{a^2(\theta^-)^2}$$

As $\lambda \to 0$, i.e., as the compressor inertial parameter decreases, $R_L \to \psi_m$. At the limit, therefore, instability onset occurs *when the pressure rise in the low inlet total pressure sector reaches the uniform flow instability onset point*. This is precisely the criterion applied in early versions of the parallel compressor model.

Examination of Equations 11 indicates that λ only occurs in the combination λ/a. For given λ, when the characteristics have high curvature near their peak pressure rise, the predictions of the model will approach those of the parallel compressor model. An example calculation of loss of stability margin, defined in terms of pressure rise at constant speed, is shown in Figure 6 (the conditions are described in the figure caption) and it appears that the simple parallel compressor always overestimates the loss in stability margin.

The corresponding axial velocity profiles at the neutral stability case are shown for a 180° square wave in Figure 7 for different values of λ/a. The IMS = 0 criterion implies that comparable amounts of the annulus must be at negative $d\psi/d\theta$ ($\phi > \phi_m$), i.e., at conditions corresponding to locally stable operation as are at positive $d\psi/d\phi$ ($\phi < \phi_m$) corresponding to locally unstable conditions. The most interesting aspect of

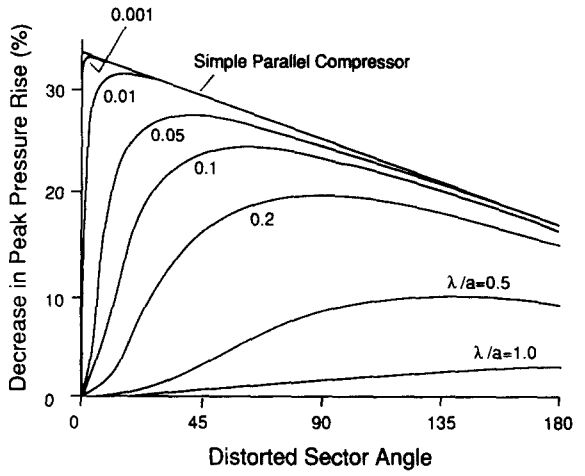

Figure 6 Effect of compressor parameter λ/a on decrease in peak pressure rise—computations based on criterion of zero integrated mean slope (IMS) at instability point and parabolic compressor characteristic, $\Delta P_t/\rho U^2 = 0.5$

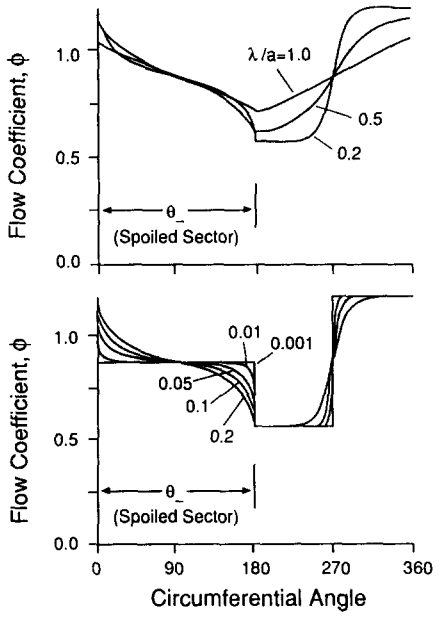

Figure 7 Local time mean compressor parameters versus circumferential position for different values of compressor parameter λ/a; 180° extent distortion and parabolic compressor characteristic

Figure 7 is the manner in which the value λ/a determines the way this balance is achieved. The (locally) least stable part of the annulus is not in phase with the low inlet total pressure (spoiled) sector and, indeed, in the limit $\lambda/a \to 0$, the high inlet total pressure (unspoiled) sector operates at two points on the axisymmetric characteristic.

The analysis given in this section shows clearly the connection between the present unsteady model and the results given by the quasi-steady simple parallel compressor model, as well as illustrating trends that are seen in practice for effect on stability. This, plus the ideas expressed in the previous section concerning the growth and decay of waves in the annulus, portray, we think, the essential fluid mechanic features determining the stability of compressors operating with inlet circumferential distortion. It is to be stressed, however, that the ideas only apply when the IMS = 0 criterion holds, and we must now examine the conditions under which this criterion must be modified.

Behavior near compressor and compression system frequency coincidence

One condition where the IMS = 0 criterion is not valid occurs when the frequency of propagating modes and system type modes coincide. Note that the system frequency referred to here is the Helmholtz frequency, rather than the small amplitude surge frequency, although for practical purposes there is very little difference between them. As was seen in Figure 3, the propagating eigenmode will have a strong zeroth harmonic component, A_0. More importantly from an applications point of view, instability occurs at a higher flow rate than would be predicted by the IMS = 0 criterion.

A typical magnitude of the effect is shown in the two curves in Figure 8, which give the throttle coefficient, K_t, at instability. One curve shows throttle coefficient at stall versus the ratio of system frequency to frequency of the propagating mode disturbance, as B is varied, keeping the compressor nondimensional length, η, constant. The second shows a corresponding plot for constant B but varying η. For reference, a 10% drop in throttle coefficient corresponds to roughly a 5% increase in flow. Figure 9 shows how the average compressor slope at instability moves towards the negatively sloped portion of the compressor

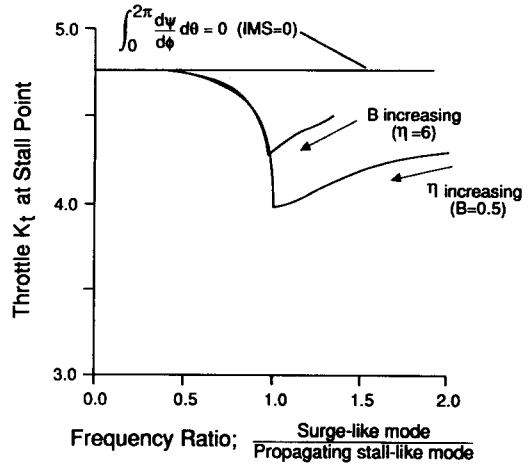

Figure 8 Effect of response (frequency coincidences) on throttle setting at stall point (instability); $\lambda = 1$, $\mu = 2$, 120° extent distortion, $\Delta P_t/\rho U^2 = 0.2$

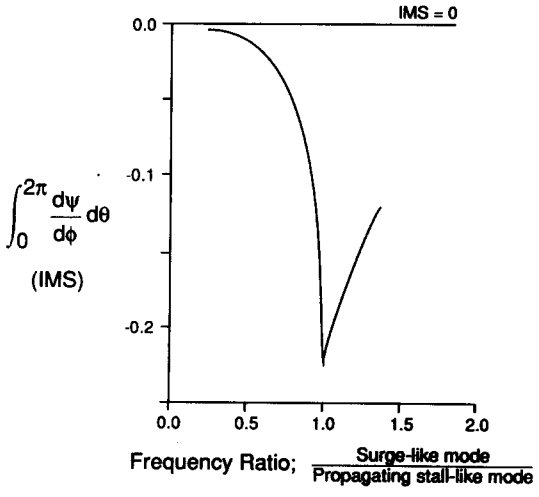

Figure 9 Variation in integrated mean slope (IMS) as a function of surge frequency/propagating disturbance (rotating stall) frequency ratio; $\eta = 6$, $\lambda = 1$, $\mu = 2$, 120° extent distortion, $\Delta P_t/\rho U^2 = 0.2$

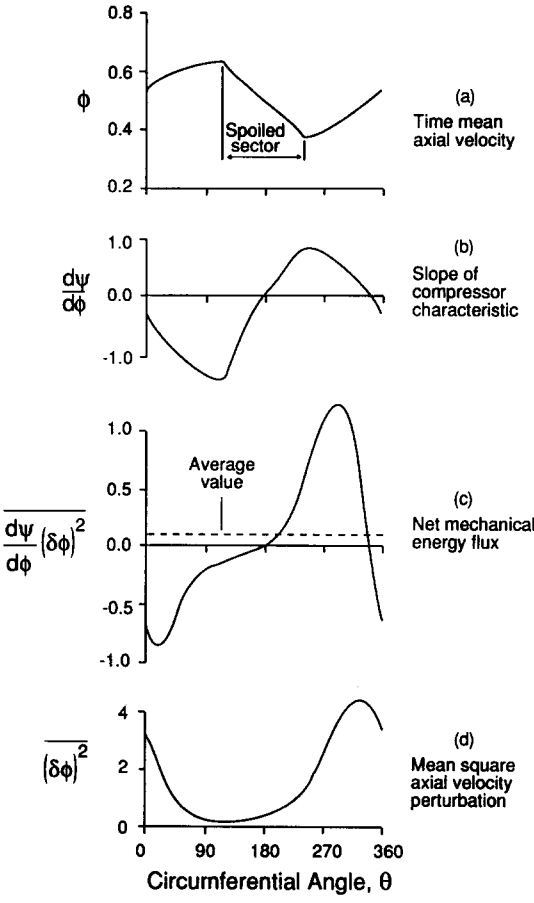

Figure 10 Circumferential distributions of mean and perturbation variables at neutral stability point near resonance; $B = 0.34$, $\eta = 6$, $\lambda = 1$, $\mu = 2$, 120° extent distortion, $\Delta P_t/\rho U^2 = 0.2$

characteristic, away from the IMS = 0 value as frequency coincidence occurs. An analytic calculation procedure for this shift in stability has recently been developed by Longley.[3]

Physical mechanism for instability at frequency coincidence

The result that there is a marked change in the instability point when the "system type" frequencies associated and the frequencies of the propagating type of disturbances approach one another is new, and we will spend some time describing the physical mechanism associated with it. The situation can be viewed as one in which the traveling wave (compressor type) perturbations create fluctuating forces which drive the system type of perturbations. This coupling of the compressor and compression system type perturbations, can occur only if there is a nonuniform flow in the compressor.

Consider the situation at neutral stability when compressor and compression system frequencies are near coincidence. The instability is due to a net mechanical energy flux out of the compressor, which is fed into the flow field perturbations. A useful simple indicator of this net mechanical energy flux is the product of the local variation in total-to-static pressure rise $(d\psi/d\phi)\delta\phi$ times the local axial velocity $\delta\phi$. Although this does not correspond exactly to the net energy flux, it is closely linked to it and, more importantly, the value of $(d\psi/d\phi)(\delta\phi)^2$ gives indication of the regions in which instability is to be expected.

Time mean circumferential variations and the disturbance eigenmode structure are given in Figure 10. Figures 10(a) and

10(b) show the time mean axial velocity distribution and the slope of the axisymmetric compressor characteristic, $d\psi/d\phi$, as a function of θ. The location of the far upstream distortion in total pressure (spoiled sector) is also indicated. The annulus averaged slope is clearly negative at this operating point.

Figure 10(c) shows the net (averaged over a period $2\pi/\omega$) value of $(d\psi/d\phi)(\delta\phi)^2$. Although the average slope of the compressor characteristic is negative, there is a net positive energy flux. For this to occur, the magnitude of the axial velocity perturbations must be considerably larger in the region of positive slope (roughly $\theta=\pi$ to $\theta=2\pi$) than in the region of negative slope. The square of the axial velocity perturbations shown in Figure 10(d) bears this out.

To understand why this occurs, let us, for the moment, represent the disturbance eigenmodes by zeroth and first harmonic components only. Computations using this representation show much the same behavior as the full representation (i.e., decreased stability in the neighborhood of the coincidence point), so such a description is very useful as a model of the more complex situation described by the full calculation. A sketch showing the relationships of these two components is given in Figure 11, which portrays different times during a cycle. The circumferential position has the same reference as that in Figure 10.

When the traveling wave part of the eigenmode is in phase with the time mean velocity profile, and thus out of phase with the slope of the axisymmetric compressor characteristic, as in the (Time 1) top plot in Figure 11, the planar component of the eigenmode has a negative velocity associated with it. When the traveling wave is out of phase with the time mean velocity (Time 3 plot), the planar component gives a positive velocity.

The effect of these phase relationships is indicated on a compressor characteristic in Figure 12. Unsteady velocity perturbations are shown for the high flow (roughly $0<\theta<\pi$) and low flow (roughly $\pi<\theta<2\pi$) regions: the nomenclature 1, 2, 3, 4 refers to the situation at the times in Figure 11. The larger filled symbols refer to a representative time mean operating point in each region, i.e., representative points on the positive and negative slopes.

At Time 1, the excursion in the low flow (positive slope) region will be larger than that in the high flow region, since both harmonic components of the eigenmode contribute a

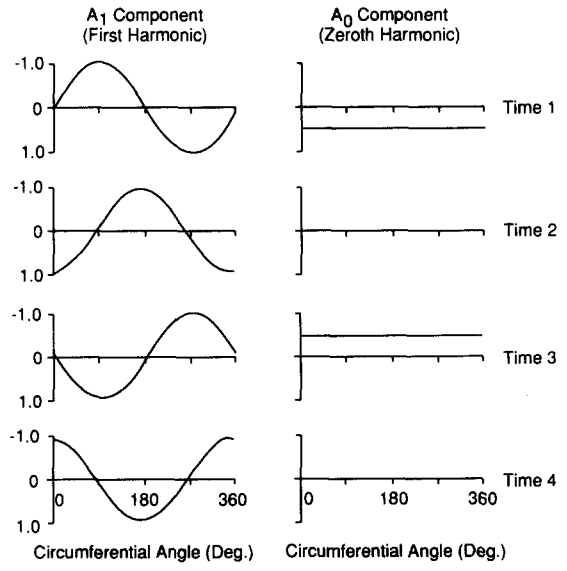

Figure 11 Sketch of zeroth and first harmonic component phase relationship; neutral stability point near resonance. Times shown differ by $\Delta t=\pi/2\omega$

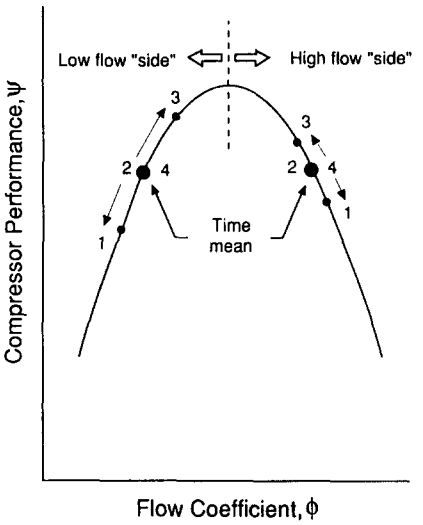

Figure 12 Local mass flow and pressure rise excursions at resonance conditions showing larger variations on low flow (positive slope) part of characteristic

negative velocity in the former. In the high flow region, the traveling wave part of the velocity is positive while the planar part is negative so the net excursion is less.

At Time 2 and Time 4 the perturbation is near zero, but at Time 3 there is again addition of velocities from the different harmonic components in the low flow region and partial cancellation in the high flow region. The phase relationships of the compressor perturbations (the traveling disturbances) and the system pulsations thus cause the velocity fluctuations in the positive sloped region to be much larger than those in the negatively sloped region.

The foregoing kinematical description shows that two circumstances must occur for decreased stability (compared to IMS=0) due to compressor/compression system complexity: the magnitude of the zeroth component must be a significant fraction of the first component, and the phase of the two components must have a relationship similar to that in Figure 11. To determine when this occurs, we examine the dynamics of the compression system.

The perturbations in annulus averaged compressor pressure rise are due mainly to the traveling wave component of the velocity disturbance. With reference to Figures 10 and 11, at Time 1, both the high flow and low flow sides have a lower pressure rise than the time mean (the flow on the low side is lower and the flow on the high side is higher; both situations lead to a decrease in the pressure rise). Conversely, at Time 3, the pressure rise is higher than the mean. At 2 and 4, the pressure rise perturbation will be close to zero. The pressure perturbations due to the zeroth harmonic component are much smaller because the annulus average is close to the peak, and the amplitude of the zeroth harmonic is smaller than that of the first harmonic. Because of this, we can consider as a good approximation only traveling wave disturbances when describing the instantaneous annulus averaged pressure rise. This latter quantity, which is essentially the axial force, will be of the form $\delta F=F_0e^{i\omega t}$ and will have its largest positive value near Time 3 and its largest negative value near Time 1.

The response of a compression system composed of a compressor, plenum, and throttle to such perturbations can be expressed in terms of a transfer function, annulus averaged mass flow fluctuation/compressor pressure rise

$$\frac{\delta\dot{m}_t}{\delta F}=\frac{1+i(\omega/\omega_H)B\tilde{T}'}{1-(\omega/\omega_H)^2+(i/B\tilde{T}')(\omega/\omega_H)} \tag{12}$$

where ω is the frequency of the traveling wave perturbation, ω_H is the overall Helmholtz system frequency, and $\bar{T}'$ is the slope of the throttle characteristic.

Equation 12 shows that the normalized compressor mass flow fluctuation will be maximized very near the point where the traveling wave frequency equals the Helmholtz frequency, i.e., very near the condition $\omega/\omega_H = 1$. Although this is not necessarily the same condition as that for the largest decrease in stability, it is to be expected that there is a close link between the two. Examination of the transfer function, as well as (A_0/A_1), the ratio of annulus averaged mass flow fluctuation (zeroth harmonic component) to the first harmonic, based on the full calculation, shows the following trends concerning phase and amplitude. The largest amplitude of the zeroth harmonic occurs at a situation in the neighborhood of frequency coincidence. For values of B larger than that corresponding to coincidence, the phase of the zeroth and first harmonics is near 90°, and the mechanism described with reference to Figures 11 and 12 will not be important. For values of B lower than coincidence, the amplitude of the zeroth harmonic decreases drastically. Thus, only in the neighborhood of coincidence where the system is essentially being driven at resonance are the proper conditions met for instability to occur on the negatively sloped part of the curve.

To recap, what has been said, and what can be seen explicitly from the form of the transfer function, the interaction between compressor type traveling wave perturbations and the flow field nonuniformity can be regarded as a forcing term for the compression system. The response of the latter is greatest at conditions of resonance, and this is where the largest effect on stability is seen. The coupling involved in the forcing depends critically on the presence of a time mean circumferential distortion, and does not occur in a uniform flow.

Rotating inlet distortions

Another instance in which the IMS = 0 criterion does not hold is for rotating distortions. There has recently been interest in this type of distortion, which propagate (rotate) at some fraction of rotor speed. One situation where this occurs is in high pressure compressors in two (or three) spool engines subjected to the distortion created by a rotating stall in the low pressure compressor.[11] Rotating distortions can be regarded as one example of the general class of dynamic distortions, with which the present analysis is capable of dealing.

Detailed experimental evidence is somewhat sparse, but one of the striking results that has been seen with rotating distortions is the strong decrease in stability if the rotation speed becomes close to the stall cell propagation speed. This was observed in Ref. 12 where an analogy with resonant behavior of a simple system was drawn, as well as in the experiments described in Ref. 13.

To examine this phenomenon, calculations have been carried out with inlet distortions rotating at various fractions of rotor speed, f, from $f = -0.6$ (against rotor rotation) to $f = 0.6$ (with rotor rotation). The background flow upstream and downstream of the compressor is taken to be steady in a frame that rotates at the distortion frequency. The equation expressing the compressure rise, Equation 1, is then

$$\frac{P_2 - P_{t_1}}{\rho U^2} = \psi(\phi) - (\lambda - \mu f)\frac{\partial \phi}{\partial \theta} \tag{13}$$

There are two important differences between Equation 13 and Equation 2 which was for steady distortion. Because the flow ahead of the compressor is unsteady, P_{t_1} is no longer simply the upstream distorted value. Changes in P_{t_1} will now arise as the result of the unsteady flow and these must emerge from a calculation of the compressor entry flow field. It should be noted that it is only the *irrotational* part of the upstream velocity field that gives rise to these (nonconvected) total pressure perturbations which, to the order of approximation adopted, obey Laplace's equation. Second, the flow downstream of the compressor is unsteady and P_2 must reflect this fact.

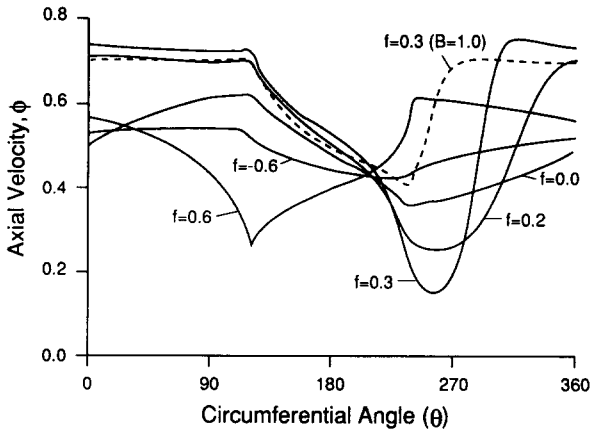

Figure 13 Effect of distortion rotation rate, f $(=\omega_{distortion} r/U)$ on background axial velocity profile at neutral stability; $\eta = 6$, $\lambda = 1$, $\mu = 2$, 120° extent distortion, $\Delta P_t/\rho U^2 = 0.2$. Solid curves are for $B = 0.01$; dashed curve is for $B = 1.0$

The solutions of Equation 13 for the background flow axial velocity distribution are shown in Figure 13 for a range of distortion rotation rates, f $(=\omega_{distortion} r/U)$. The distortion is a square wave of amplitude $\Delta P_t/\rho U^2 = 0.2$ and extent 120°. All calculations represent conditions at the neutral stability point corresponding to that particular rotation rate. The calculations have been done for a constant far upstream total pressure distortion as measured in the frame of reference fixed to the distortion. The solid lines denote conditions for a very low value of B (0.01) far from any compressor/compression system frequency coincidence. The dotted line shows the behavior for $f = 0.3$ and a larger value of $B = 1.0$; this will be described subsequently.

There are large differences between the curves, and some of the reason for this can be seen from Equation 13. The coefficient of $\partial\phi/\partial\theta$ in Equation 13 changes as f is varied. When $f = -0.6$, it is more than double the value for $f = 0$. This amounts to an effective increase of the inertia parameter which shows directly in the reduced distortion in axial velocity. When $f = 0.6$, the coefficient of $d\phi/d\theta$ has opposite sign to the steady value. Very loosely, this is analogous to changing the sign of $\partial\phi/\partial\theta$, and the form of the ϕ curve thus roughly mirrors image of the steady $(f = 0)$ value.

One cannot focus attention solely on the coefficient $\lambda - \mu f$, however, since the pressure terms in Equation 13 are also important. A complete analysis shows that the relevant term is of the form $\lambda - (\mu + 2/|k|)f$; this indicates increased sensitivity when the distortion rotation rate is near stall propagation rate. (Note that the extent of the increased sensitivity will also depend on the shape of the compressor characteristic, through the parameter λ/a). The axial velocity profiles at the compressor inlet for values of $f = 0$ and 0.3, also shown in Figure 13, bear this out. At a value of $f = 0.3$, close to the stall cell speed, the velocity profile has a large amplitude. At this condition, the inlet distortion is forcing the compressor at frequencies that are close to those of the natural eigenmodes (the frequency of stall cell propagation), so that a larger response might be expected.

This is also seen in the overall compressor pressure rise characteristics plotted in Figure 14. The axisymmetric curve is

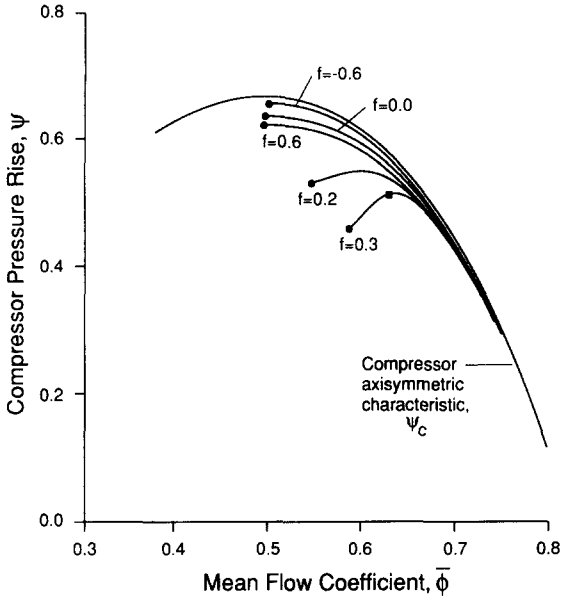

Figure 14 Effect of distortion rotation rate, f ($=\omega_{distortion}r/U$) on overall compressor performance; $\eta=6$, $\lambda=1$, $\mu=2$, 120° extent distortion, $\Delta P_t/\rho U^2=0.2$. Solid circles show neutral stability points for $B=0.01$, solid square indicates neutral stability point for $B=1.0$

shown as well as distorted flow characteristics for the same rotation speeds as in Figure 13. The distorted flow characteristics are plotted up to the neutral stability point, i.e., the curves terminate at instability. Because an actual distortion would scale roughly as ϕ^2 and the calculations have been done with a constant value of $\Delta P_t/\rho U^2$, the figure underestimates somewhat the degree to which the performance at higher flows is degraded at distortion rotation rates which are near the natural stall cell speed. As distortion rotation rate is increased from zero to 0.3, the figure shows a drop in the compressor performance (due to the increase in axial velocity nonuniformity) and a shift in the stall point. In particular, for $f=0.3$, there is only a small regime in which the flow is stable.

In common with the case of steady distortion, the parts of the annulus which are most likely to promote unstable perturbations, i.e., the low flow regions, are to be found *outside* the sector having low inlet total pressure. Attempts to investigate what determines the stall point must thus model the fluid dynamic coupling of the spoiled and unspoiled sectors, and an approach based only on total pressure patterns and any type of "critical residence time" is not adequate to do this.

Compressor/compression system coupling with rotating distortions

The compressor/compression system coupling and the decrease in stability due to rotating distortion have been presented so far as separate phenomena, but the two can also interact with one another. The combination of an imposed rotating distortion plus the naturally propagating disturbance creates annulus averaged perturbations at a frequency set by the *difference* of the rotation rates of the former and the latter. This difference frequency can also come into coincidence (resonance) with the system modes.

For the compressor and system that has been discussed, we found that, for a stationary distortion, coincidence is computed to occur near $B=0.35$. Thus, consider the behavior at a value of B far from this, say $B=1$, as the rotation rate of the distortion is increased from initially zero. As the distortion rotation rate increases, the difference between distortion rotation and stall propagation frequencies will decrease and approach the system frequency. The result will be a tendency towards decreased stability. For the present situation, the magnitude of the effect is illustrated by the shift in instability point from the solid circle (for $B=0.01$) to the solid square (for $B=1.0$) in Figure 14.

There is, of course, a general trend towards decreased system stability as B is increased, and it is difficult to disentangle this from the effect of coincidence. The main point is clear, however —most of the positively sloped portion of the distorted flow compressor characteristic can be unstable for moderate (or larger) values of B, and stable flow range and performance with rotating distortion can be severely affected.

As a final note on this aspect, we can compare the axial velocity distribution at the neutral stability point for the rotating distortion, $f=0.3$, for the two values of B, 0.01 and 1.0. The latter is given by the dashed line in Figure 13. At the lower value there is little coupling with the system and the strong response of the compressor to the rotating distortion is seen. In this case, instability can be regarded as due to the flow local to the compressor. At the higher value, the interaction with the system causes instability at a much higher flow rate, and the region of strong distortion/compressor eigenmode resonance cannot be accessed.

Effect of loss modeling on stability prediction

In analyzing the effects of inlet distortion, there have been a number of approaches to modeling the unsteady blade response which is an important part of the problem. All of these, at least for multistage compressor models, are quite rudimentary when compared to the actual situation. As part of the present investigation, we thus examine the impact of the choice of model on predictions of the analysis.

In the preceding sections, the losses and exit angles were assumed to follow blade row inlet flow variations quasi-steadily, so that the unsteady effects included only an inertia term. In this section, we relax this assumption and let the instantaneous loss across a blade row lag the incidence changes, as determined by

$$\frac{\tilde{\tau}_L r}{U}\frac{dL}{dt}=L_{SS}-L \tag{14}$$

where L is a loss coefficient, and L_{SS} is the steady state value of the loss coefficient at the instantaneous flow condition. The nondimensional time constant, $\tilde{\tau}_L$, has been shown to have a value approximately equivalent to the time necessary for a particle to convect through a blade row,[14] so that

$$\tilde{\tau}_L \cong \frac{b_x U}{C_x r} \cong 0.1\text{–}0.3$$

for typical compressor parameters.

If the distortion is steady, the equation replacing Equation 2 which describes the steady background flow becomes

$$\frac{P_2-P_{t_1}}{\rho U^2}=\psi_{ID}-L_S-L_R-\lambda\frac{d\phi}{d\theta} \tag{15}$$

where ψ_{ID} is an "ideal" pressure rise characteristic, based on actual flow angles and zero loss. ψ_{ID} and the stator loss, L_S, are functions of ϕ only. The term L_R represents the sum of the losses through the rotors and is found from the solution of

$$\tilde{\tau}_L\frac{dL_R}{d\theta}=L_{R_{SS}}-L_R \tag{16}$$

assuming similar rotors for each stage.

For small values of the left-hand side (recall $\tau_L \cong 0.1$–0.3), to first order we can write

$$L_R = L_{R_{SS}} - \tilde{\tau}_L \left(\frac{dL_{R_{SS}}}{d\phi}\right)\left(\frac{d\phi}{d\theta}\right) \tag{17}$$

Substituting Equation 17 into Equation 15, we obtain an equation analogous to Equation 2:

$$\frac{P_2 - P_{t_1}}{\rho U^2} = \psi(\phi) - \lambda_{eff}\frac{d\phi}{d\theta} \tag{18}$$

where ψ_{ID}, L_S and $L_{R_{SS}}$ have been regrouped to form ψ and

$$\lambda_{eff} = \lambda - \tilde{\tau}_L \frac{dL_{R_{SS}}}{d\phi} \tag{19}$$

Equation 19 can be regarded as defining an effective λ; the utility of this is discussed just below.

To illustrate the effect of the unsteady losses, Figure 15 shows the axial velocity profiles at neutral stability for a 180° square wave distortion. Three curves are shown calculated using: (a) the simple inertia unsteadiness model (as in the preceding sections), (b) the unsteady loss model, and (c) the inertia model with an appropriate value of λ_{eff}. It can be seen that, at least as far as the steady axial velocity profile is concerned, extending the blade row model to include unsteady losses is closely equivalent to increasing the value of λ.

Given the similarity between axial velocity profiles, it is not surprising that the calculated stability onset point found for the unsteady loss model and the effective λ model are similar. There is, however, a significant difference in the modes that are predicted to become unstable. The inclusion of an unsteady loss model means that, near stall, the instantaneous slope of the compressor characteristic is less positive than with quasi-steady losses. This effect increases as the degree of unsteadiness increases. This can be seen qualitatively by reference to Equation 14. For small harmonic disturbances, this becomes for rotors

$$\delta L = \frac{\delta L_{SS}}{1 + i\tau_L(\omega r/U + n)}$$

which decreases with increasing harmonic number n.

The harmonic-dependent decrease in loss variation will separate the points of instability of the eigenmodes, and this would not be predicted just from increasing the effective λ. Figure 16 shows a quantitative illustration of the dependence on harmonic number. The first eigenmode becomes unstable

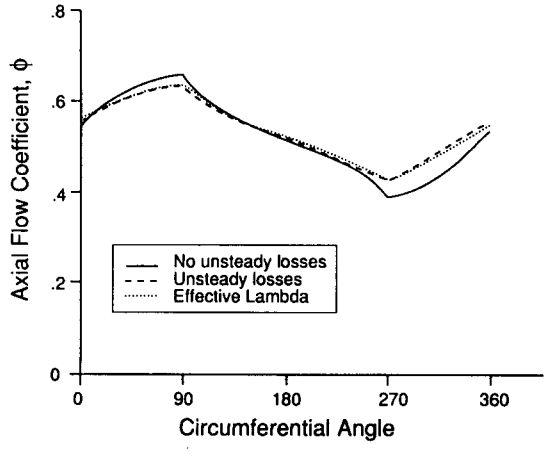

Figure 15 Effect of unsteady losses on time mean axial velocity profile at neutral stability; $B=1$, $\eta=6$, $\lambda=1$, $\mu=2$, 120° extent distortion, $\Delta P_t/\rho U^2 = 0.2$

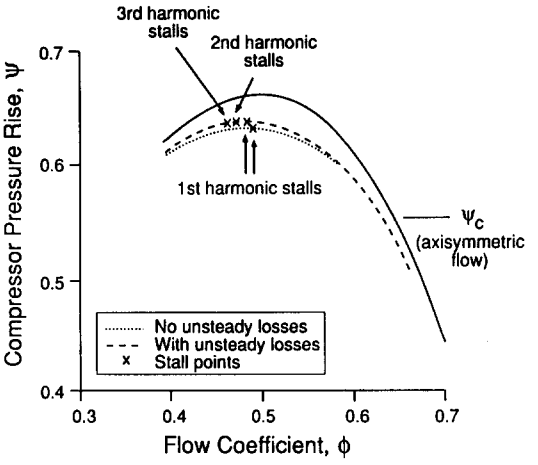

Figure 16 Effect of unsteady losses on overall compressor performance in distortion and instability point; $B=1$, $\eta=6$, $\lambda=1$, $\mu=2$, 120° extent distortion, $\Delta P_t/\rho U^2 = 0.2$

first, followed by the second, etc. Over a representative range of parameters, however, the condition at which the first mode becomes unstable is quite close to that computed using quasi-steady losses. Inclusion of unsteady losses does not, therefore, have a major effect on predicted stall point. The main effect is that higher order modes are now predicted to be more stable so that the first mode is the one that is of most import.

Summary and conclusions

(1) A fluid dynamic stability analysis has been used to examine several phenomena associated with inlet distortion in multistage axial compressors.

(2) The regimes of validity of the approximate distorted flow instability criterion

$$\int_0^{2\pi} \frac{d\psi}{d\phi}\, d\theta = 0$$

have been examined. It is shown that this is valid except near coincidence of surge (system) type frequencies and compressor (stall cell) type propagating frequencies or where the distortion is rotating at a rate near the natural frequency of a compressor propagating eigenmode. Further, the use of this criterion allows one to show clearly that the basic parallel compressor stability criterion is recovered as a limiting case of the present analysis.

(3) A rotating disturbance, whose propagation speed is close to that of the natural eigenmodes of the compressor, can cause rotating stall at a considerably higher flow rate than a disturbance that rotates with speed far from the natural value. This is in agreement with (the sparse) experimental results. In general, counterrotating disturbances are less adverse than corotating disturbances.

(4) In the neighborhood of coincidence between system (surge-like) frequencies and compressor (propagating stall-like) frequencies, there is also a decrease in stability compared to regimes where these frequencies are quite different. This is due to resonance between system and compressor perturbations, and only occurs if there is a nonuniform flow in the compressor.

(5) The inclusion of pitch average models of unsteady losses in a computation of steady-state distorted flow has an effect very similar to that of an increase in the inertial unsteady terms, and thus appears not to introduce any new fluid mechanic effects.

(6) The simple inertia lag model does not distinguish a most unstable disturbance except near resonance conditions. Inclusion of unsteady losses, however, does separate the stability points of the different modes, with the result that the first (propagating) mode is the most unstable, and hence most important to consider.

Acknowledgments

T. P. Hynes and E. M. Greitzer wish to acknowledge the NATO travel grant that made this collaboration possible. They also would like to thank Mr. D. D. Williams for many useful suggestions and for all his encouragement. The work at MIT was supported by grant NSG-3208 from the NASA Lewis Research Center, Mr. F. Newman project manager, which the authors gratefully acknowledge. Support for the visit of J. P. Longley to MIT was provided by the Ernst Zimmerman Memorial Award and by the Aircraft Engine Group, General Electric Company.

References

1 Hynes, T. P. and Greitzer, E. M. A method for assessing effects of inlet flow distortion on compressor stability. *ASME J. Turbomachinery* 1987, **109**, 371–379

2 Moore, F. K. A theory of rotating stall of multistage compressors, Parts I–III. *ASME J. Eng. Gas Turbines and Power* 1984, **106**, 313–336

3 Longley, J. P. Inlet distortion and compressor stability. Ph.D. Dissertation, Cambridge University Engineering Department, 1988

4 Longley, J. P. and Hynes, T. P. Stability of flow through multistage axial compressors. ASME Paper 89-GT-311. To be published in *ASME J. Turbomachinery*

5 Koff, S. G. and Greitzer, E. M. Axisymmetrically stalled flow performance for multistage axial compressors. *ASME J. Turbomachinery* 1986, **108**, 216–223

6 Mazzawy, R. S. Multiple segment parallel compressor model for circumferential flow distortion. *ASME J. Eng. Power* 1977, **99**, 228–246

7 Adamczyk, J. J. Unsteady fluid dynamic response of an isolated rotor with distorted inflow. AIAA Paper 74-49, 1974

8 Moore, F. K. Stall transients of axial compression systems with inlet distortion. *J. Propulsion and Power* 1986, **2**, 552–562

9 Peyret, R. and Taylor, T. D. *Computational Methods for Fluid Flow*, Springer-Verlag, 1983

10 Greitzer, E. M. The stability of pumping systems—the 1980 Freeman Scholar Lecture. *ASME J. Fluids Eng.* 1981, **103**, 193–243

11 Schaffler, A. and Miatt, D. C. Experimental evaluation of heavy fan–high pressure compressor interaction in a three-shaft engine, Parts I and II. ASME Papers 85-GT-173 and 85-GT-222, 1985

12 Ludwig, G. R., Nenni, J. P. and Arendt, R. H. Investigation of rotating stall in axial flow compressors and the development of a prototype stall control system. Technical Report USAF-APL-TR-73-45, 1973

13 Kozarev, L. A. and Federov, R. M. Aspects of the appearance and elimination of breakaway in an axial-flow compressor in the presence of a rotating non-uniformity at the inlet. *Izevstinya vuz Aviatsionnaya Tekhnika* 1983, **26**(1), 33–37 (translated)

14 Nagano, S., Machida, Y., and Takata, H. Dynamic performance of stalled blade rows. Japan Soc. Mech. Eng. Paper #JSME 11, presented at Tokyo Joint International Gas Turbine Conference, 1971

Appendix: Description of compressor and flow field modeling

Compressor performance

The basic equation describing compressor performance, Equation 1, is derived under the following assumptions. The (low speed) compressor is taken to be of sufficiently high hub-to-tip ratio that a two-dimensional description of flow through it can be used. Provided all flow disturbances of interest have a circumferential wavelength much greater than a blade pitch, one can sensibly define a local value of incidence onto a blade row at each circumferential location. It is assumed that, at each θ, a blade row performs as it would in uniform flow at the local value of incidence (i.e., it produces the same pressure rise, loss, turning, etc.) apart from an additive, unsteady correction to account for the inertia of the fluid in the blade row.

If all the unsteady pressure rise across a blade row is balanced by local inertia effects, then

$$\Delta P|_{\mathrm{UNS}} = -\frac{\rho b}{\cos\gamma}\left(\frac{\partial W}{\partial t}\right)_{\mathrm{rel}} \tag{A1}$$

In this equation, b is the blade chord, γ is the stagger angle, and W is the relative velocity. The time rate of change is taken in a coordinate system fixed to the particular blade row of interest. Thus, for a rotor, we have

$$\Delta P|_{\mathrm{UNS}} = -\frac{\rho b}{\cos\gamma}\left(\frac{\partial W}{\partial t}+\frac{U}{r}\frac{\partial W}{\partial \theta}\right) \tag{A2}$$

in the absolute system.

If crossflow in the small gaps between blade rows is neglected, conservation of mass implies that axial velocity is continuous at each θ across a blade row (and in fact across the whole compressor) so that

$$\frac{W}{U}=\frac{\phi}{\cos\gamma} \tag{A3}$$

where ϕ is the inlet (and exit) flow coefficient ($\phi = C_x/U$) at that θ. Each blade row is assumed to have a turning which depends only on the local, instantaneous value of incidence, so the incidence that each blade row sees (apart from the first) will be a function only of ϕ at that particular value of θ.

Under these conditions, the local static pressure rise across the ith stage is

$$\frac{\Delta P}{\rho U_i^2} = F_i(\phi) - \tau_{\mathrm{R}_i}\left(\frac{\partial\phi}{\partial t}+\frac{U}{r}\frac{\partial\phi}{\partial\theta}\right) - \tau_{\mathrm{S}_i}\frac{\partial\phi}{\partial t} \tag{A4}$$

where $\tau = b/\cos^2\gamma$, the subscripts R and S refer to rotor and stator, respectively, and F_i is the pressure rise in axisymmetric flow at the local value of ϕ. The compressor is taken as having a row of inlet guide vanes, so that Equation A4 is valid for each stage of the compressor.

The inlet guide vanes themselves must be treated slightly differently since it is no longer true that local values of incidence are a function only of local values of flow coefficient in an asymmetric flow. We assume instead that the flow through the IGVs consists of loss-free turning at the leading edge and then unsteady blade channel flow. A similar expression to Equation A1 results for the pressure rise, but involving the total pressure at inlet,

$$\frac{P_{\mathrm{out}}}{\rho U^2} - \frac{P_{t_{\mathrm{in}}}}{\rho U^2} = F_{\mathrm{IGV}}(\phi) - \tau_{\mathrm{IGV}}\frac{\partial\phi}{\partial t} \tag{A5}$$

The performance for the compressor as a whole is then obtained by adding Equation A4 for each stage to Equation A5, to obtain

$$\frac{P_2 - P_{t_1}}{\rho U^2} = \psi(\phi) - \lambda\frac{\partial\phi}{\partial\theta} - \frac{\mu r}{U}\frac{\partial\phi}{\partial t} \tag{A6}$$

where $\psi = \sum F_i + F_{\mathrm{IGV}}$ is the undistorted compressor performance characteristic. The parameters λ and μ represent the

inertia of the fluid in the rotor and stator passages and are given by

$$\lambda=\sum_{i=1}^{N}\tau_{R_i}\frac{U}{r} \tag{A7}$$

and

$$\mu=\left[\sum_{i=1}^{N}(\tau_{R_i}+\tau_{S_i})+\tau_{IGV}\right]\frac{U}{r} \tag{A8}$$

Equation A6 is Equation 1. It applies throughout the paper except for the next-to-last section, which examines the effect of relaxing some of the assumptions concerning the unsteady flow in the blade row.

Flow fields external to the compressor

Equation A6 can only be solved if some way of relating P_2 and P_{t_1} to ϕ is added. The required relationships are found by considering the dynamics of the upstream and downstream flow fields. It is argued that a simplified description of these is adequate and, in particular, that the flow external to the compressor can be described by a two-dimensional, inviscid set of equations linearized about a uniform flow. The details of how this is done differ slightly accordingly to whether the inlet distortion is steady or unsteady, and what follows is a description applicable to the steady distortion case.

Upstream of the compressor, the flow field linearization implies, for the steady, distorted background flow, that the upstream reaction of the compressor is a potential flow. The total pressure distribution is thus the same function of θ at the compressor face as it is at upstream infinity. (For the unsteady perturbation, used to determine the stability of the background flow, the flow field linearization assumption implies again that the desired relationship between δP_{t_1} and $\delta\phi$ required by Equation 3 is that applicable to an unsteady potential flow.)

Downstream of the compressor, it is assumed that the compressor discharges axially into an annular duct which is several mean radii long, and then into a plenum before throttling. The axial momentum and continuity equations for this region are:

$$-\frac{1}{\rho}\frac{\partial P'}{\partial x}=\frac{\partial C_x'}{\partial t}+\bar{C}_x\frac{\partial C_x'}{\partial x} \tag{A9}$$

and

$$\frac{\partial C_x'}{\partial x}+\frac{1}{r}\frac{\partial C_\theta'}{\partial\theta}=0 \tag{A10}$$

At compressor exit, if the compressor is sufficiently heavily bladed, $C_\theta'=0$, and hence $\partial C_\theta'/\partial\theta=0$ there. The continuity equation A10 then implies that at compressor exit $\partial C_x'/\partial x=0$, so that Equation A9 reduces to

$$\left[-\frac{1}{\rho}\frac{\partial P'}{\partial x}=\frac{\partial C_x'}{\partial t}\right]_{\text{at compressor exit}} \tag{A11}$$

The axial velocity perturbation at the compressor C_x'/U, can be written quite generally as

$$\frac{C_x'}{U}=\sum_{-\infty}^{\infty}a_k e^{ik\theta+i\omega t}$$

The downstream static pressure variations are irrotational (satisfying $\nabla^2 P'=0$) so that P' must be of the form

$$\frac{P'}{\rho U^2}=\left(\sum_{n\neq 0}\alpha_k e^{ik\theta-|k|x/r}+\alpha_0\frac{x}{r}+\beta_0\right)e^{i\omega t} \tag{A12}$$

The assumption that the exit ducting is several radii long ensures that only the decaying exponentials need be included in Equation A12. The boundary condition A11 determines the α_n in terms of the a_n and so provides the required relationship between static pressure variations downstream of the compressor and local axial velocity variations.